JOURNAL OF SPACECRAFT AND ROCKETS
Vol. 33, No. 5, September–October 1996

High-Enthalpy and Perfect-Gas Heating Measurements on a Blunt Cone

Brian R. Hollis* and John N. Perkins†
North Carolina State University, Raleigh, North Carolina 27695-7921

Detailed aerodynamic heating measurements were made on a 70-deg sphere-cone configuration model and in the wake of the model on the sting. Tests were conducted in hypersonic flows in a high-enthalpy impulse facility, in which air and carbon dioxide were employed as test gases, and in a conventional perfect-gas air wind tunnel. Heating data were also obtained on three similar parametric forebody configurations. Normalized forebody Stanton number distributions were independent of Reynolds number and test gas, with the exception of smaller forebody corner heating peaks in carbon dioxide. Peak wake Stanton numbers were 5% of the forebody stagnation point values in the high-enthalpy tests and varied with Reynolds number from 7 to 15% of the stagnation point values in the perfect-gas tests. The impulse facility wake flow establishment process was studied in detail, and a criterion for determining when the wake flow becomes established was developed. Wake flow establishment was found to require on the order of 45–75 flow-path lengths as based on the model size and freestream velocity.

Nomenclature

C = $\mu^* T_\infty / \mu_\infty T^*$
C_H = Stanton number, $q/[\rho_\infty U_\infty (h_0 - h_w)]$
c_p = specific heat, J/kg-K
h = enthalpy, J/kg
k = thermal conductivity, W/m-K
L = surface distance along sting from model base, m
Q = heat energy, J/m^2
q = heat transfer rate, W/m^2
Re = Reynolds number, $\rho U x/\mu$
R_b = forebody base radius, m
S = surface distance measured from the stagnation point, m
T = temperature, K
T^* = reference temperature, $(T_{0,2}/6)[1 + (3T_w/T_{0,2})]$, K
t = time, s
U = velocity, m/s
y_{ref} = reference length for flow establishment
α = thermal diffusivity, $k/\rho c_p$, m^2/s
β = thermal product, $\sqrt{(k\rho c_p)}$, W-s$^{1/2}$/m^2-K
λ = heat transfer correction factor, 1/K
Δ = uncertainty bound for a parameter
μ = viscosity, kg/m-s
μ^* = viscosity evaluated at T^*, kg/m-s
ρ = density, kg/m^3
σ = heat transfer residual for flow establishment
τ = nondimensional flow establishment time, $U_\infty \Delta t / y_{\text{ref}}$

Subscripts

w = wall conditions
0 = total or stagnation conditions
0, 2 = post-normal-shock stagnation conditions
2 = post-normal-shock static conditions
∞ = freestream conditions

Introduction

SEVERAL Mars exploration missions are now being planned by NASA, the first of which is the Mars Pathfinder[1] probe (formerly known as MESUR). In the design of planetary entry vehicles such as Mars Pathfinder, data on heat transfer rates on the forebody are essential in the determination of heat-shielding requirements, and characterization of the behavior of the flow in the wake of the vehicle is an important factor in payload size and placement. The purpose of this study was to generate a database of forebody and wake heating measurements on a configuration based on the Mars Pathfinder spacecraft for use in the design of future such vehicles as well as for use in computational fluid dynamics code comparison exercises. These measurements were made in both high-enthalpy and perfect-gas flows. To interpret the high-enthalpy data, it was also necessary to determine a method for characterizing the wake flow establishment process in an impulse facility.

Heat-Transfer Test Models

The focus of this study was on heat-transfer measurements on a 70-deg sphere-cone configuration similar to the Mars Pathfinder vehicle. A limited parametric study was also conducted by measuring heating rates on three similar configurations. The four configurations that were tested are shown in Fig. 1, and the dimensions of the models are given in Table 1.

The primary configuration that was tested was a 70-deg sphere-cone geometry with a nose radius to corner radius ratio of 10 and a 40-deg cone-frustrum afterbody. This configuration is similar to that of the Mars Pathfinder vehicle and will be referred to as MP–1. The other three configurations had different forebody geometries but had the same afterbody as MP–1. The MP–2 configuration was a hyperboloid with the same nose radius-of-curvature and forebody base diameter as MP–1, whereas the MP–3 and MP–4 configurations were 70-deg sphere-cones with corner radii that were two and four times, respectively, the corner radius of MP–1. All four configurations had a forebody base radius R_b of 2.54 cm and were supported in the test facilities on identical stings of 0.406 forebody base radii and of approximately 4.5 forebody base radii length.

Heat-transfer test models of each of the four configurations were fabricated from Macor® (Corning Glass Works), a machinable, thermally insulative, glass-ceramic material, and were instrumented with thin-film temperature resistance gauges following the procedure described in Ref. 2. Each model was equipped with

Table 1 Dimensions of heat-transfer test models

Model	R_b, cm	R_n/R_b	R_f/R_b	R_c/R_b	W/R_b	R_s/R_b	L_s/R_b Mach 10	L_s/R_b HYPULSE
MP–1	2.54	0.5	0.6	0.05	0.862	0.406	5.250	4.625
MP–2	2.54	N/A	0.6	0.05	0.834	0.406	5.250	4.625
MP–3	2.54	0.5	0.6	0.10	0.915	0.406	5.200	4.620
MP–4	2.54	0.5	0.6	0.20	1.021	0.406	5.200	4.620

Received Aug. 2, 1995; revision received April 1, 1996; accepted for publication May 26, 1996.

*Graduate Research Assistant, Mechanical and Aerospace Engineering Department. Member AIAA.
†Professor, Mechanical and Aerospace Engineering Department. Associate Fellow AIAA.

Table 2 Operating conditions of test facilities and uncertainty estimates

FACILITY	M_∞	U_∞, m/s	$Re_\infty \cdot 10^{-6}$, 1/m	p_∞, Pa	ρ_∞, kg/m^3	T_∞, K	$P_{t,2}$, kPa	$T_{t,2}$, K	$h_0 - h_{298}$, MJ/kg	ρ_2/ρ_∞
31-Inch Mach 10	9.68 ±0.0%	1416 ±0.2%	1.621 ±1.7%	69.0 ±1.1%	0.00451 ±1.4%	53.3 ±0.4%	8.38 ±1.2%	1008 ±0.3%	0.75 ±0.5%	5.97 ±0.0%
31-Inch Mach 10	9.80 ±0.1%	1422 ±0.3%	3.187 ±1.1%	130.6 ±0.5%	0.00868 ±0.7%	52.5 ±0.8%	16.3 ±0.5%	1015 ±0.6%	0.76 ±1.0%	5.98 ±0.1%
31-Inch Mach 10	9.93 ±0.0%	1425 ±0.2%	6.198 ±0.9%	242.0 ±0.4%	0.01646 ±0.7%	51.5 ±0.8%	31.0 ±0.5%	1017 ±0.3%	0.77 ±0.5%	5.99 ±0.0%
HYPULSE, CO_2	9.71 ±4.1%	4772 ±1.1%	0.660 ±4.9%	1191 ±10%	0.00571 ±1.8%	1088 ±8.7%	129.6 ±1.8%	3703 ±0.9%	12.25 ±2.1%	18.98 ±1.0%
HYPULSE, Air	7.93 ±4.1%	5162 ±1.1%	0.668 ±3.9%	1824 ±9.9%	0.00579 ±3.1%	1113 ±9.3%	147.2 ±1.3%	6028 ±0.8%	14.18 ±1.4%	10.98 ±0.7%

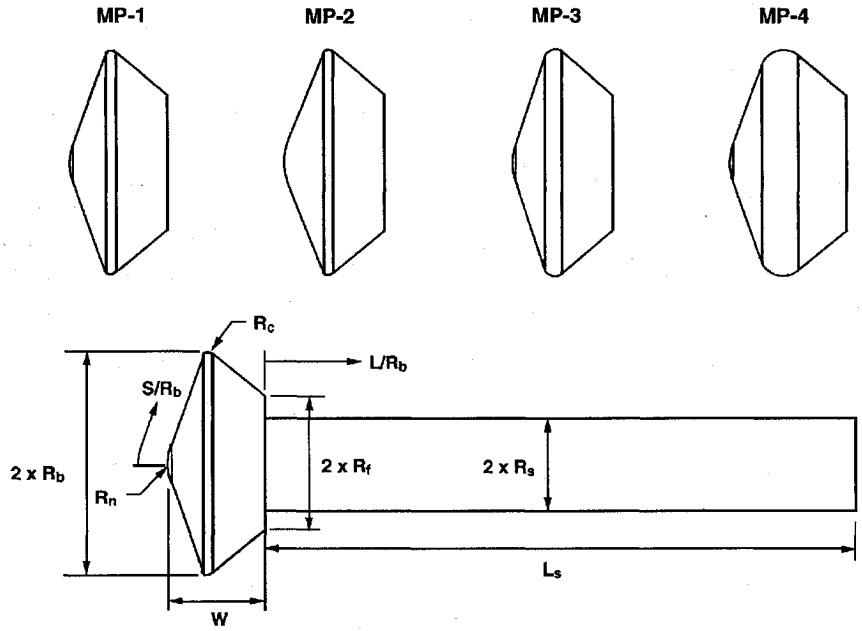

Fig. 1 Heat-transfer test model configurations.

37 thin-film gauges located along a single ray that covered both the forebody and afterbody of the model. Stings for the models were fabricated from stainless steel. A slot was machined in each sting for a contoured Macor insert with an additional 33 thin-film gauges. Gauge spacing on the models and stings was approximately 2.5 mm.

Test Facilities

Aerodynamic heating tests were conducted in two hypersonic research facilities: the 31-Inch Mach 10 Air Tunnel[3] at the NASA Langley Research Center, and the NASA HYPULSE[4] Expansion Tube, which is operated by the General Applied Sciences Laboratories (GASL). The 31-Inch Mach 10 facility is a conventional blowdown, low-enthalpy, hypersonic wind tunnel. This facility has a large test core (~14-in. diam), high flow uniformity (~1% pitot pressure deviation across the test core), and, for a conventional facility, a high temperature driver potential (1000 K reservoir temperature). Test times in the 31-Inch Mach 10 Air Tunnel for this study were 3–5 s, although longer test times are possible for aerodynamic studies, and data were sampled at a rate of 50 Hz. The HYPULSE Expansion Tube is a 6-in.-diam impulse facility in which steady, high-enthalpy, hypervelocity flows are produced in which minimal freestream test gas dissociation occurs. The HYPULSE Expansion Tube can be operated with a number of different gases, although in this study only CO_2 and air were employed. HYPULSE test times for this study were on the order of 100–200 μs, and the data sampling rate was 500 kHz.

Nominal flow conditions for these facilities are given in Table 2. Uncertainty estimates given in this table for run-to-run repeatability of the test conditions are defined by the 95% confidence level of two standard deviations[5] of the individual values, as determined statistically from the flow properties measurements made during all of the tests in this research. The flow properties uncertainty in the Mach 10 facility was estimated to be no more than ±1% for any of the properties, whereas for HYPULSE the uncertainties in the individual flow properties were estimated to vary from ±1 to ±10%.

Data Reduction

Surface heat-transfer rates were computed from measured thin-film gauge temperature-time histories using both classical closed-form analytical methods and a numerical method. The first analytical method was the classical, one-dimensional, constant thermal properties, semi-infinite solid method developed by Cook[6]:

$$q(t_n) = \frac{2\beta}{\sqrt{\pi}} \sum_{i=1}^{i=n} \frac{T_i - T_{i-1}}{\sqrt{t_n - t_i} + \sqrt{t_n - t_{i-1}}} \tag{1}$$

The method of Eq. (1) is referred to as the direct method. Heating rates were also computed using the indirect method developed by Kendall et al.[7] and Hedlund et al.[8] in which the heating rate is computed from the time derivative of the total heat added as a function of time:

$$Q(t_n) = \frac{\beta}{\sqrt{\pi}} \sum_{i=1}^{i=n} \frac{(T_i - T_1) + (T_{i-1} - T_1)}{\sqrt{t_n - t_i} + \sqrt{t_n - t_{n-1}}} \Delta t \tag{2a}$$

$$q(t_n) = \frac{dQ_n}{dt} = \frac{-2Q_{i-8} - Q_{i-4} + Q_{i+4} + 2Q_{i+8}}{40\Delta t} \tag{2b}$$

The assumption is made in the development of both the direct and indirect methods that the thermal properties of the model substrate material do not vary with temperature. In fact, the thermal properties of Macor do exhibit a dependence on temperature. The curve fits for Macor thermal properties[9] used in this research are

$$\rho = 2543\ (\text{kg/m}^3) \tag{3a}$$

$$k = 0.33889 + 7.4682 \times 10^{-3} \times T - 1.6118 \times 10^{-5} \times T^2 + 1.2376 \times 10^{-8} \times T^3\ (\text{W/m-K}) \tag{3b}$$

$$\alpha = 1.3003 \times 10^{-6} - 2.2523 \times 10^{-9} \times T + 1.8571 \times 10^{-12} \times T^2\ (\text{m}^2/\text{s}) \tag{3c}$$

The uncertainty in these curve fits is estimated to be on the order of ±5%.

To account for these variations in thermal properties with temperature, an empirical correction factor λ for the thermal product β was derived for Macor in a manner similar to that discussed in Ref. 2. This parameter can be used to correct the heat transfer rates computed using either Eq. (1) or Eq. (2) by

$$\dot{q}_{\text{var}} = \dot{q}_{\text{const}}(1 + \lambda \Delta T_w) \tag{4a}$$

where

$$\lambda = 7.380 \cdot 10^{-4} - 4.603 \cdot 10^{-7} \Delta T_w \tag{4b}$$

and

$$\Delta T_w = T_w - 298\ \text{K} \tag{4c}$$

The validity of this empirical correction was confirmed by comparison with results obtained from the numerical technique, which is an implicit, one-dimensional finite volume model of the heat conduction within the model substrate. The temperature dependencies of the bulk material properties (k and α) are directly accounted for in this numerical discretization. The difference between the finite volume results and the results from the empirically corrected direct or indirect method results was found to be on the order of 2% over the range of surface temperatures encountered ($300\ \text{K} < T < 450\ \text{K}$) in these tests.

The 1DHEAT data reduction code, which incorporates this numerical technique and the two analytical methods, was used to perform all heat-transfer computations. The 1DHEAT code is detailed in Ref. 9, in which a more detailed discussion of the data reduction techniques and additional information on Macor thermal properties and the derivation of the correction factor are presented.

In this research, the analytical methods were used for rapid, initial reduction of the data, and these calculations then were verified later using the finite volume method. With respect to the analytical methods, the use of the indirect method was preferred over that of the direct method, as it tended to produce a clearer representation (with less noise) of the heat-transfer time-history, especially in regard to the wake flow establishment process. This is because at discrete sample times the temperature-difference term in the numerator of Eq. (1) tends to accentuate fluctuations in the heating rate, whereas the temperature-sum in the numerator of Eq. (2a) and the wide differencing stencil in Eq. (2b) tend to smooth fluctuations. However, both the direct and indirect methods do yield nearly identical time-averaged heating rates over a given time interval. The differences in the results from these two methods are illustrated in Fig. 2, in which the heat-transfer time histories of the stagnation point gauge on the MP–1 model as calculated by the two methods for a test in the 31-Inch Mach 10 tunnel are shown. In regard to the choice of the indirect method over the direct method, note that the direct method might be more applicable in situations in which the dynamic behavior of the heating rates is of interest, such as in turbulent or unsteady flow, as high-frequency dynamic behavior can be damped by the indirect method. This damping was not a concern in the analysis of the wake flow establishment process, as only the averaged values of final established flow heating rates were of interest.

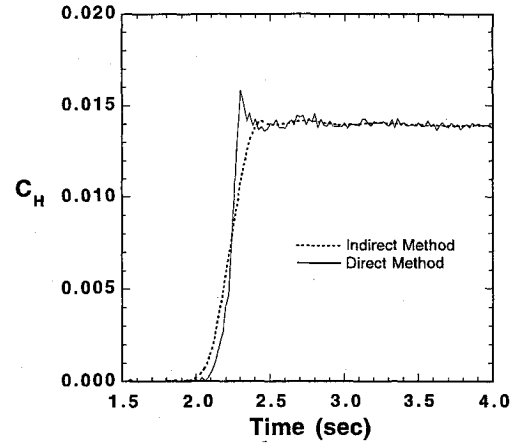

Fig. 2 Comparison of direct and indirect method heat-transfer computations.

Heating data from these tests will be presented in the form of Stanton numbers to eliminate the effect of the increasing model surface temperature on the heat-transfer rates during the test period. Because of the short test time in HYPULSE and the lower total temperature in the Mach 10 tunnel, this model surface temperature increase was only on the order of 100–150 K. Because of this, lateral conduction effects in the model could be neglected, and so, with allowances for experimental noise, the Stanton number distributions on the models remained effectively constant over time. Thus, for comparison with computational fluid dynamics results, dimensional heat-transfer rates can be extrapolated back to values at a specified surface temperature within this range from the Stanton number. With respect to computational simulations, note that Macor is considered to be a noncatalytic material.

Stanton Number Uncertainty Estimates

The Stanton numbers cited herein represent the time averages of the values determined from the computed heat-transfer rates and measured surface temperatures during the steady test flow time-window of the respective facility. The two standard deviation uncertainty bands for the 95% confidence level of the heat-transfer rates over the time-averaging windows were approximately ±1% on the forebody and ±3% in the wake for 31-Inch Mach 10 Air Tunnel tests and approximately ±10% on the forebody and ±15% in the wake for HYPULSE Expansion Tube tests. Wake uncertainties were higher than on the forebody because the measured heat fluxes in the wake were an order of magnitude lower than on the forebody, which made them more sensitive to disturbances from freestream fluctuations or electrical noise.

The overall Stanton number uncertainty can be estimated by taking into account the contributions from the measured heating rates, the thermal properties, and the freestream conditions (all of which have a linear effect on the computation and are assumed to be independent) by

$$\Delta_{\text{tot}} = \sqrt{\Delta_q^2 + \Delta_{\text{Macor}}^2 + \Delta_\rho^2 + \Delta_U^2 + \Delta_{\Delta h}^2} \tag{5}$$

This computation gives an uncertainty estimate of ±5% for the forebody Stanton number and ±6% for the wake for the 31-Inch Mach 10 Air Tunnel tests, with the primary influence on the computation being the uncertainty in Macor thermal properties. For the HYPULSE tests, the Stanton number uncertainty estimate is ±12% for the forebody and ±16% for the wake, with the dominant factor being the effect of experimental noise on the measurement of the dimensional heat transfer rates.

Results and Discussion

Each of the four configurations were tested in both the 31-Inch Mach 10 Air Tunnel and in the HYPULSE Expansion Tube. In the Mach 10 tunnel, the MP–1 configuration was tested at zero angle of attack at freestream unit Reynolds numbers of 1.62, 3.19,

and 6.20×10^6 m^{-1}at a constant total enthalpy level of 0.7 MJ/kg (relative to enthalpy fixed at zero at 298 K). The MP–1 configuration was also tested at angles of attack from −4 to −20 deg. Each of the parametric configurations was tested at the 3.19×10^6 m^{-1} Reynolds number condition. In HYPULSE, each configuration was tested in CO_2 at a freestream unit Reynolds number of 0.66×10^6 m^{-1} with a 12.3 MJ/kg enthalpy level. The MP–1 and MP–2 configurations were tested in air in HYPULSE with a freestream unit Reynolds number of 0.67×10^6 m^{-1} and a 14.2 MJ/kg enthalpy level.

Stanton number surface distributions are plotted vs S/R_b, which is the distance from the geometric center of the forebody normalized by the forebody base radius, or vs L/R_b, which is the normalized distance along the sting from the base of the model. Because the afterbody and sting Stanton numbers were one or two orders of magnitude lower than on the forebody, the Stanton numbers plots have two y axes, one for the forebody values and one for the wake values.

31-Inch Mach 10 Air Tunnel Results

Reynolds number effects on the MP–1 configuration are shown in Fig. 3, in which C_H is normalized by the measured stagnation point value. The local maximum occurring at $S/R_b \sim 1.7$ corresponds to the location of afterbody corner. Although the Reynolds number had little effect on the normalized forebody distributions, a significant increase in the normalized Stanton number and a movement of the wake peak toward the model base with Reynolds number were observed. The peak sting value was 15% of the stagnation point value at the 6.20×10^6 m^{-1} freestream Reynolds number, 11% at 3.19×10^6 m^{-1}, and 8% at 1.62×10^6 m^{-1}. This increase with Reynolds number is not thought to be attributable to transitional or turbulent behavior of the wake shear layer because of the relatively low freestream Reynolds numbers and the small size (5.08 cm maximum diameter) of the test models. Furthermore, attempts to trip the boundary-layer flow by applying fine grit to the forebody of the model produced no change in the wake heating behavior, which suggests that the flow was normally laminar and that even if the forebody flow was tripped by the grit, it relaminarized at the corner expansion fan or in the shear layer.

Stanton number distributions for the MP–1 configuration at angles of attack of 0, −4, −12, and −20 deg are presented in Fig. 4. As expected, changing the angle of attack increased the peak wake heating value and moved its location inward toward the base of the model. The peak value was 11% of that at the geometric stagnation point (i.e., at the symmetry axis) at zero deflection and increased to 36% at the maximum deflection of −20 deg. On the forebody, the angle of attack had minimal effect on the geometric stagnation point Stanton number value but had a large effect on the corner values, where the peak windward corner value at the maximum deflection was nearly equal to that at the geometric stagnation point.

Forebody and wake Stanton number distributions for MP–1 and the parametric configurations at $Re_\infty = 3.19 \times 10^6$ m^{-1} are shown in Fig. 5. Configuration effects were negligible on the forebody except for the lower stagnation region Stanton numbers (~10% lower at the stagnation point) that were produced by the blunter nose of the hyperboloid MP–2 configuration. Away from the nose, the MP–2 C_H distribution asymptotically approached that of the sphere-cone

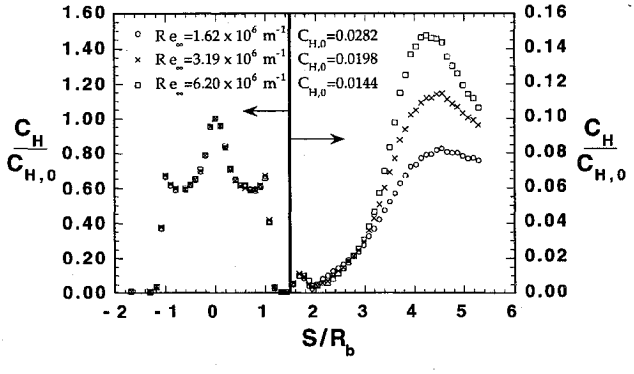

Fig. 3 Reynolds number effects on MP–1 configuration in 31-Inch Mach 10 Air Tunnel.

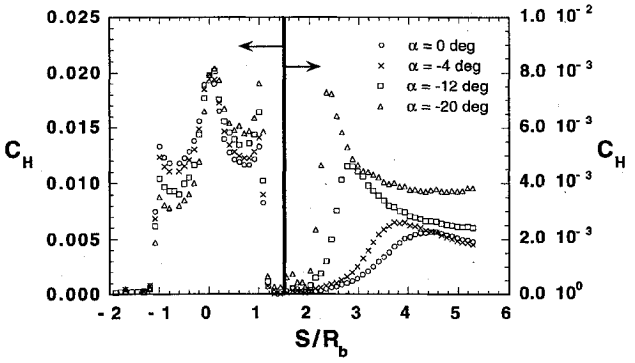

Fig. 4 Angle-of-attack effects on MP–1 configuration in 31-Inch Mach 10 Air Tunnel, $Re = 3.19 \times 10^6$ m^{-1} test condition.

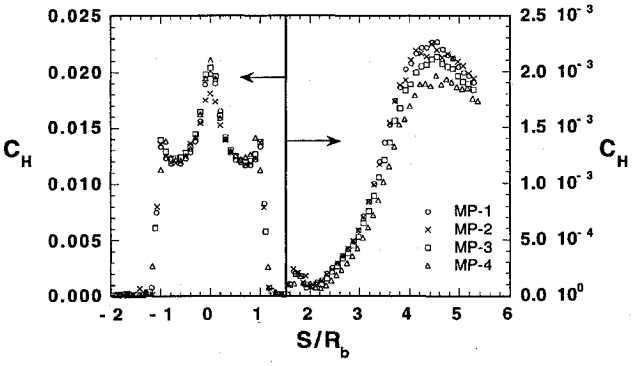

Fig. 5 Configuration effects in 31-Inch Mach 10 Air Tunnel, $Re = 3.19 \times 10^6$ m^{-1} test condition.

configurations just as its hyperboloid geometry approaches that of the sphere cones. For this reason, the MP–1 and MP–2 afterbody and sting distributions were essentially identical. The measured Stanton numbers on the sting for MP–3 and MP–4 were, respectively, approximately 8 and 13% lower than those for MP–1 and MP–2. This is most likely a result of the shear layer being accelerated less in turning around the larger corner radii of these of configurations. As a percentage of their respective stagnation point values, the peak sting Stanton numbers were approximately 11% of the stagnation point value for MP–1, 12% for MP–2, 10% for MP–3, and 9% for MP–4.

Wake Flow Establishment in HYPULSE

Before presenting the data from HYPULSE, the subject of wake flow establishment must be addressed. This establishment process is important because the time required for a wake flow to become fully established, although negligible in relation to test times in a conventional wind tunnel, can represent a significant portion of the available test time in an impulse facility. During this establishment process, wake heating distributions can vary rapidly over a wide range of values before a steady, established distribution is reached. To determine the correct wake heating values, the measured time histories of the heat transfer rates must be carefully studied, and their behavior must be related to both the wake establishment process and the operating characteristics of the facility.

In HYPULSE, the duration of a test is dictated by the length of time between the arrival of the incident shock wave and the arrival of the unsteady expansion fan. This test window was determined by examination of wall pressure data (model size prevented simultaneous use of a pitot probe) recorded at the exit of the expansion tube. Within this total test window, a criterion of ±5% maximum variation in the wall pressure was used to determine the length of time during which valid data on the wake establishment process could be obtained. On average, this test sub-window was found to be approximately 150 μs for CO_2 and approximately 120 μs for air. These times are more conservative than those generally quoted for HYPULSE.[4] However, it was observed that, owing to the extremely small surface temperature rise (1–5 K as opposed to 50–100 K on

the forebody) and consequentially low heating on the afterbody and sting, the wake Stanton numbers were extremely sensitive to freestream flow fluctuations. Furthermore, the ±5% pressure variation criterion reduces the freestream properties uncertainty level, which lends more credibility to the use of these data for comparisons with computational results. For these reasons, these more conservative test times were used to bound the window over which the Stanton numbers could be averaged. However, note that well-behaved forebody heating rates data were obtained over longer time intervals, which approached the nominal HYPULSE test times of 200–300 μs.

After fixing the maximum test time by the preceding method, it was then necessary to determine at what point within this window the wake flow became fully established. In the past, flow establishment often was determined by analysis of pressure or heating time history data from individual gauges. The flow at a given point was said to be established when the measured values reached some percentage (for example 95%) of their mean values. However, because the mean values could not be known beforehand, this approach could be subject to interpretation. Furthermore, these established values could be reached at different times for different locations on the model, which made this method of analysis more complicated. For these reasons, it was decided that a global method was required for determining when the flow became established throughout the entire wake region.

Initially, plots of heating rate vs position along the sting were generated at each discrete time during the test at which data were recorded. A computer slide show "movie" of these distributions was then generated using commercially available software. These motion pictures provided a graphical illustration of the establishment process, and the point at which the heating distributions stabilized throughout the wake could usually be clearly identified. A hard-copy analog of one such movie is presented in Figs. 6a–6d in which heating distributions along the sting at several times are overlaid on a single plot. In the period immediately after the incident shock arrival, the heating rates fluctuated rapidly as the forebody flow and the outer inviscid core of the wake were established (Fig. 6a). The fluctuations dampened, and then the heating distribution began to gradually approach a steady state as the flow in the recirculation region immediately behind the base was established (Fig. 6b). The distribution then reached a steady-state value (Fig. 6c), where it remained until the expansion fan arrived, which ended the test period (Fig. 6d).

Although a valuable qualitative analytical tool, the motion picture approach was without a theoretical or mathematical basis for determining an establishment criterion. Also, as Figs. 6a–6d illustrate, the presentation of a movie in a static format is somewhat difficult. A criterion for wake flow establishment with more quantitative foundations was derived through the use of a normalized heat transfer residual defined by

$$\sigma(t) = \Delta q/q \tag{6a}$$

where

$$\Delta q = \frac{\partial q}{\partial t}\Delta t \tag{6b}$$

This residual can be used to represent the establishment process because, as the wake flow approaches established behavior, the heating rates approach constant values and thus the residuals approach zero (note that in HYPULSE the heating rates are approximately constant because the wall temperature increase is negligible with respect to the stagnation temperature).

To characterize the entire wake region, a root-mean-square (rms) variation was computed from the residual time histories of the individual gauges in the wake by

$$\mathrm{rms}(\sigma) = \sqrt{(1/n)\left(\sigma_1^2 + \sigma_2^2 + \cdots + \sigma_n^2\right)} \tag{7}$$

To isolate the wake flow establishment process from variations as a result of freestream flow fluctuations or electrical noise, the heat flux time derivative was computed with a differencing formula of the form of Eq. (2b). Furthermore, gauges that were producing noisy data because of gauge damage or poor electrical contacts were removed from this computation as the noise tended to mask the details of the establishment process.

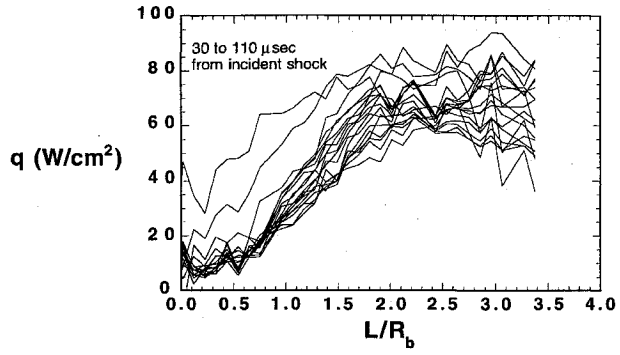

Fig. 6a Wake establishment movie: flow establishing.

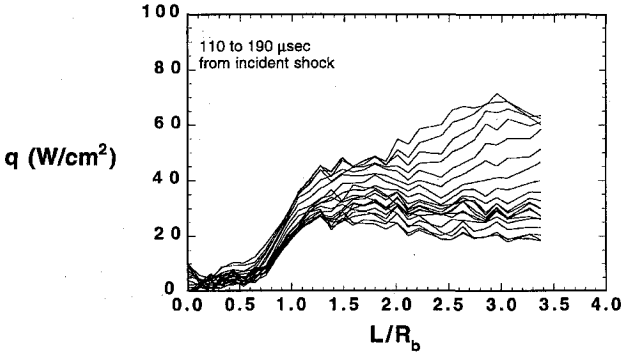

Fig. 6b Wake establishment movie: flow establishing.

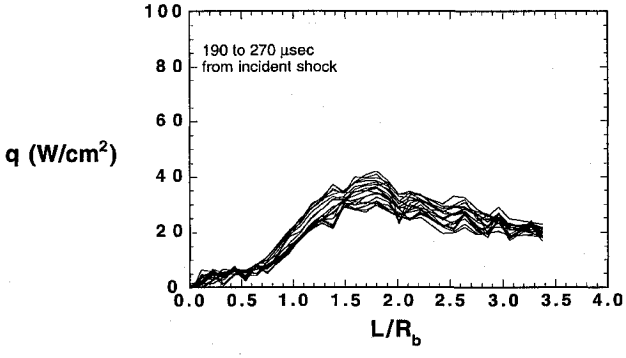

Fig. 6c Wake establishment movie: established flow.

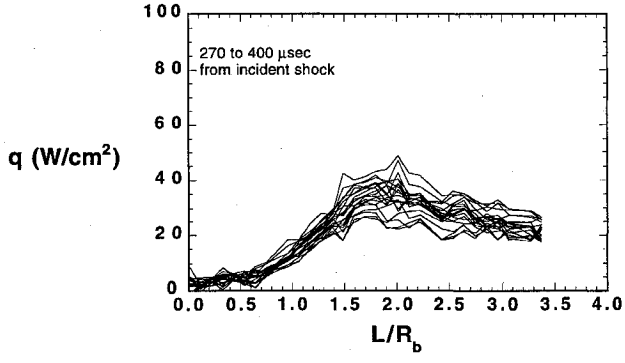

Fig. 6d Wake establishment movie: unsteady expansion fan.

In general, it was observed that the wake heating rms was initially extremely high because of the arrival of the incident shock and the forebody flow establishment process (which required on the order of 50 μs from the arrival of the incident shock) and then tended toward zero as the wake flow was established. This behavior can

be seen in Fig. 7 in which the rms time history of the same test depicted in Figs. 6a–6d is presented. The incident shock arrival, the establishment of the recirculation region of the wake, and the arrival of the expansion fan can all be seen in this rms time history. Analysis of the data led to an establishment criterion of rms(σ) ~ 0.02 for the wake flow being set. This value was in part determined by observation of the rms values at the times at which the motion pictures showed that the heating distributions were constant.

Based on the times determined from the rms approach, the nondimensional establishment parameter was computed from

$$\tau = \frac{U_\infty t_{\text{est}}}{y_{\text{ref}}} \tag{8}$$

In this case, the reference dimension y_{ref} was taken to be the difference between the model forebody base radius R_b and the sting radius. The establishment parameter values fell between 45 and 75 for both the air and CO_2 tests, and the average value of τ was 67 in air and 56 in CO_2. These values are consistent with previous results[10] and fell within the available HYPULSE test times. In fact, these values may be slightly better than those in Ref. 10 since the reference dimension apparently was taken to be the body radius in that work, as opposed to the difference between the body and sting radii.

HYPULSE Expansion Tube Results

Stanton number distributions for the MP–1 configuration in CO_2 and air test gases are presented in Figs. 8 and 9. Owing to the somewhat greater uncertainty level in the HYPULSE tests, distributions from repeat runs are shown. In CO_2, the local corner heating peak appears to have been too narrow to be resolved with the gauge spacing on the models (computational results do predict a peak, for example, Ref. 11), whereas the peak is clearly indicated in the air data. Peak sting C_H values in both air and CO_2 were approximately 5% of the stagnation point values. Note that the freestream Reynolds number for both air and CO_2 tests in HYPULSE was 0.66×10^6 m^{-1}, which is less than half of the lowest Reynolds number in the Mach 10 tests, and so the wake shear layer again was assumed to remain laminar.

Configuration effects on the Stanton number distributions in CO_2 and air are shown in Figs. 10 and 11. Although the stagnation region

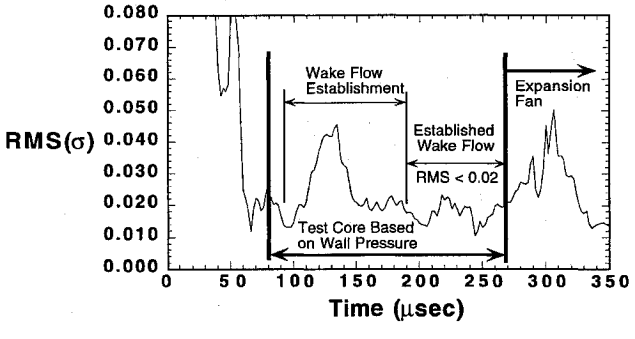

Fig. 7 Wake-establishment rms time history.

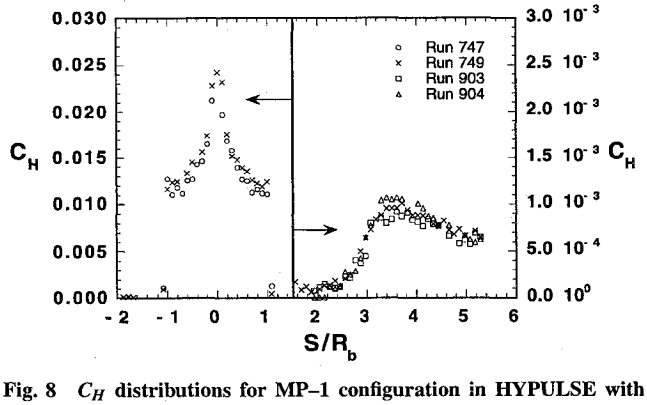

Fig. 8 C_H distributions for MP–1 configuration in HYPULSE with CO_2 test gas.

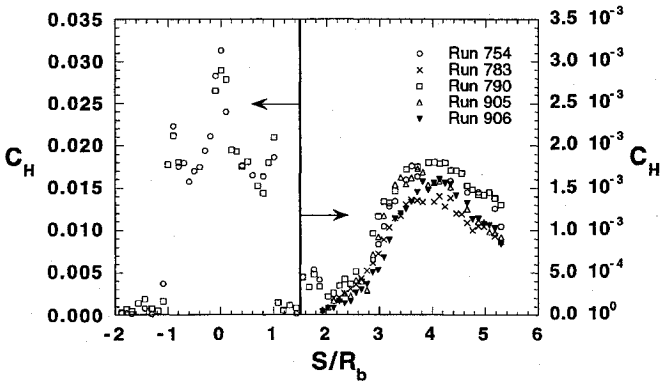

Fig. 9 C_H distributions for MP–1 configuration in HYPULSE with air test gas.

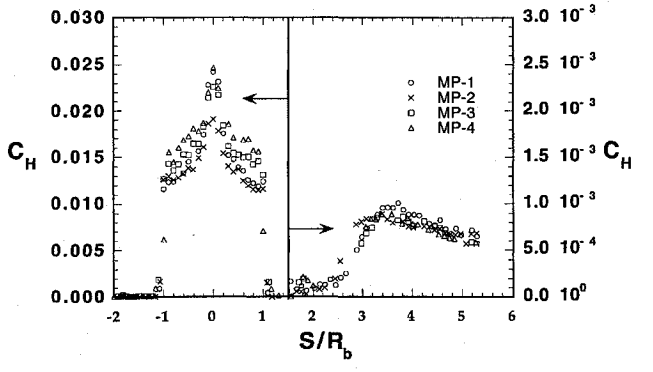

Fig. 10 Configuration effects in HYPULSE with CO_2 test gas.

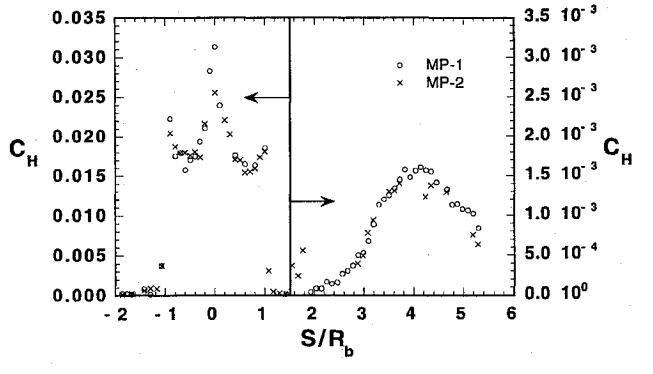

Fig. 11 Configuration effects in HYPULSE with air test gas.

Stanton numbers for the three sphere-cone configurations (MP–1, 3, and 4) were all within the repeatability of the data for the CO_2 tests, the larger corner radii MP–3 and MP–4 configurations exhibited anomalously higher heating (on the order of 10%) along the conical portions of the forebodies. As in the Mach 10 tests, the blunter stagnation region of the MP–2 hyperboloid again led to lower stagnation region Stanton numbers. The hyperboloid stagnation point value was approximately 20% lower than that of MP–1 for both air and CO_2. Configuration effects on the wake distributions were very slight, although the data seem to indicate a small decrease in peak sting Stanton number with increasing corner radii. Peak sting C_H values in CO_2 were approximately 5% of the stagnation point values for MP-1, 6% for MP–2, 4% for MP–3, and 3% for MP–4. In air, the peak sting values were 5% for MP–1 and 6% for MP–2.

Comparison of Mach 10 and HYPULSE Results

Stanton number distributions for HYPULSE were correlated as suggested in Ref. 12 in terms of the viscous interaction parameter, $M_\infty(C^*/Re_\infty)^{1/2}$, and the shock density ratio, ρ_2/ρ_∞. However, although the density ratio was raised to the one-quarter power in that work, it was found that the high-enthalpy data from HYPULSE correlated better with the two-thirds power and that this also served to correlate the perfect-gas Mach 10 data.

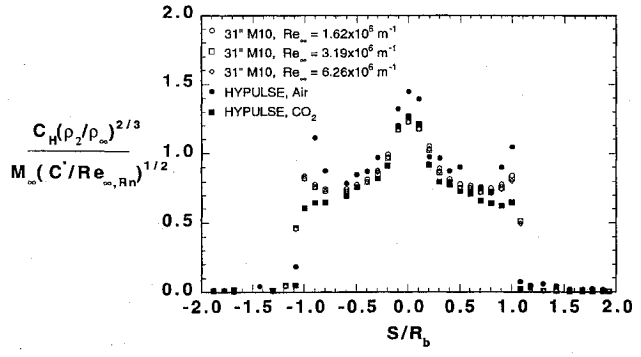

Fig. 12 Correlated forebody distributions.

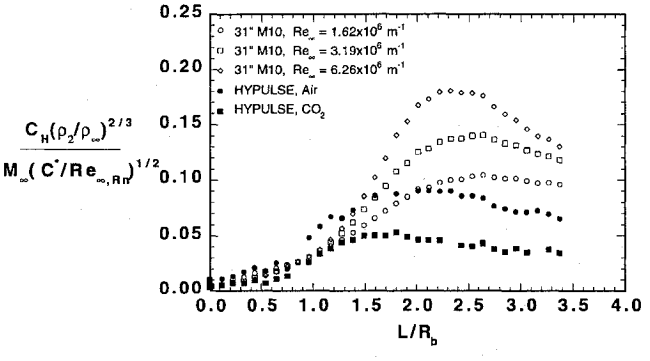

Fig. 13 Correlated wake distributions.

The correlation parameter distributions for the forebody and wake are shown in Figs. 12 and 13. The forebody distributions for both the HYPULSE air tests and for the different Reynolds numbers of the Mach 10 air tests correlated very well, although the CO_2 distribution exhibited less of a corner peak than the air tests. In the wake, the peak sting value decreased nearly linearly with Reynolds number and moved away from the body in the Mach 10 tests. However, in both HYPULSE test gases, the location of the peak was much closer to the body and was of greater magnitude than the trend of the Mach 10 data would suggest. As flowfield chemistry did not appear to have a large effect on the correlated forebody distributions, this difference is attributed to vibrational nonequilibrium produced in the rapid expansion of the flow around the forebody corner.

Conclusions

A 70-deg sphere-cone entry vehicle model and three similar parametric configurations were tested in a high-enthalpy, hypervelocity impulse facility and in a conventional wind tunnel. Detailed aerothermodynamic measurements were made on the models and on instrumented stings in the wakes of the models. Forebody Stanton number distributions for all four configurations were similar; however, the hyperboloid configuration Stanton number was lower near the stagnation point, whereas the larger corner radii sphere-cone configurations exhibited slightly higher heating along their conical flanks. Wake Stanton numbers were one to two orders of magnitude lower than forebody stagnation point values. In the 31-Inch Mach 10 Air Tunnel, the peak wake Stanton number varied with Reynolds number (at a constant enthalpy level of 0.7 MJ/kg) to from 7 to 15% of the forebody stagnation point value. In the HYPULSE Expansion Tube, the values were 5% of the stagnation point in air at a 14-MJ/kg enthalpy level and 5% in CO_2 at a 12-MJ/kg enthalpy level, where the Reynolds number was 0.66×10^6 m^{-1} in both cases.

The wake flow establishment process was studied, and a method to characterize the establishment based on the rms of the heating rate residual was developed. HYPULSE tests times were found to be sufficient for flow establishment. The nondimensional establishment time varied from 45–75, with the establishment in CO_2 taking slightly less time than in air.

Acknowledgments

This work was supported by NASA Grants NAGW-1331 and NAG-1-1663 to the North Carolina State University Mars Mission Research Center. Funding for model construction and experimental testing was provided by the Aerothermodynamics Branch, NASA Langley Research Center. The authors wish to thank John Calleja of the General Applied Sciences Laboratory for his assistance in this work.

References

[1]Hubbard, G. S., Wercinski, P. F., Sarver, G. L., Hanel, R. P., and Ramos, R., "A Mars Environmental Survey (MESUR)—Feasibility of a Low Cost Global Approach," International Astronautical Federation, IAF Paper 91-432, Paris, France, Oct. 1991.

[2]Miller, C. G., "Comparison of Thin-Film Resistance Heat-Transfer Gages with Thin-Skin Transient Calorimeter Gages in Conventional Wind Tunnels," NASA TM 83197, Dec. 1981.

[3]Micol, J. R., "Hypersonic Aerodynamic/Aerothermodynamic Testing Capabilities at Langley Research Center: Aerothermodynamic Facilities Complex," AIAA Paper 95-2107, June 1995.

[4]Tamago, J., Bakos, B., Pulsonetti, M., and Erdos, J., "Hypervelocity Real Gas Capabilities of GASL's Expansion Tube (HYPULSE) Facility," AIAA Paper 90-1390, June 1990.

[5]Anon., "Assessment of Wind Tunnel Data Uncertainty," AIAA Rept. S-071, 1995.

[6]Cook, W. J., "Unsteady Heat-Transfer to a Semi-Infinite Solid with Arbitrary Surface Temperature History and Variable Thermal Properties," Mechanical Engineering Dept., Iowa State Univ., TR ISU-ERI-AMES-675000, Ames, IA, Feb. 1970.

[7]Kendall, D. N., Dixon, W. P., and Schulte, E. H., "Semiconductor Surface Thermocouples for Determining Heat-Transfer Rates," *IEEE Transactions on Aerospace and Electronic Systems*, Vol. AES-3, No. 4, 1967, pp. 596–603.

[8]Hedlund, E. R., Hill, J. A. F., Ragsdale, W. C., and Voisinet, R. L. P., "Heat-Transfer Testing in the NSWC Hypervelocity Wind Tunnel Using Co-Axial Surface Thermocouples," Naval Surface Warfare Center, NSWC MP 80-151, Silver Spring, MD, March 1980.

[9]Hollis, B. R., "User's Manual for the One-Dimensional Hypersonic Experimental Aero-Thermodynamic (1DHEAT) Data Reduction Code," NASA CR 4691, Aug. 1995.

[10]Holden, M. S., "Establishment Times of Laminar Separated Flows," *AIAA Journal*, Vol. 9, No. 11, 1971, pp. 2296–2298.

[11]Mitchletree, R. A., and Gnoffo, P. A., "Wake Flow About a MESUR Mars Entry Vehicle," AIAA Paper 94-1958, June 1994.

[12]Miller, C.G., Micol, J. R., and Gnoffo, P. A., "Laminar Heat-Transfer Distributions on Biconics at Incidence in Hypersonic, Hypervelocity Flows," NASA TP 2213, Jan. 1985.

J. C. Adams
Associate Editor